nature nanotechnology

LETTERS

PUBLISHED ONLINE: 27 MARCH 2017 | DOI: 10.1038/NNANO.2017.27

Revealing the reaction mechanisms of Li-O_2 batteries using environmental transmission electron microscopy

Langli Luo[1], Bin Liu[2], Shidong Song[2,3], Wu Xu[2], Ji-Guang Zhang[2] and Chongmin Wang[1]*

The performances of a Li-O_2 battery depend on a complex interplay between the reaction mechanism at the cathode, the chemical structure and the morphology of the reaction products, and their spatial and temporal evolution[1–4]; all parameters that, in turn, are dependent on the choice of the electrolyte[5–8]. In an aprotic cell, for example, the discharge product, Li_2O_2, forms through a combination of solution and surface chemistries[9–11] that results in the formation of a baffling toroidal morphology[12–15]. In a solid electrolyte, neither the reaction mechanism at the cathode nor the nature of the reaction product is known. Here we report the full-cycle reaction pathway for Li-O_2 batteries and show how this correlates with the morphology of the reaction products. Using aberration-corrected environmental transmission electron microscopy (TEM) under an oxygen environment, we image the product morphology evolution on a carbon nanotube (CNT) cathode of a working solid-state Li-O_2 nanobattery[16] and correlate these features with the electrochemical reaction at the electrode. We find that the oxygen-reduction reaction (ORR) on CNTs initially produces LiO_2, which subsequently disproportionates into Li_2O_2 and O_2. The release of O_2 creates a hollow nanostructure with Li_2O outer-shell and Li_2O_2 inner-shell surfaces. Our findings show that, in general, the way the released O_2 is accommodated is linked to lithium-ion diffusion and electron-transport paths across both spatial and temporal scales; in turn, this interplay governs the morphology of the discharging/charging products in Li-O_2 cells.

A functioning solid-state Li–O_2 nanobattery was constructed by taking advantage of the capability of the aberration-corrected environmental transmission electron microscope to allow *in situ* experiments in an O_2 gas environment (Fig. 1a). The experimental settings enable *in situ* atomic-level imaging and electron-diffraction analysis of the phase formed on discharging and charging of the battery. CNTs dressed with a nanosized RuO_2 catalyst were used as a cathode (Supplementary Fig. 1), Li metal as an anode and Li_2O, formed on the surface of Li metal, as a solid electrolyte. The oxygen-gas environment around the sample cell was maintained at a constant pressure of 0.1 mbar throughout the experiments. In contrast to most other Li–O_2 closed cells, in which liquid electrolytes were used, our experimental conditions correspond to the oxygen-rich working environment of a real battery.

During the discharging and charging of the solid-state Li–O_2 battery, the reaction product features a reversible formation of hollow spherical particles. The morphological evolution of the discharged product was monitored by a series of time-resolved scanning TEM high-angle annular dark-field images (Fig. 1b and Supplementary Movie 1). The bright colour contrast clearly shows the whole process: after an incubation time of a few seconds, two hollow spheres pop out at the site of the three-phase junction (the contact point of the CNTs, Li_2O/Li and O_2), followed by a continuous growth of the hollow spheres, from an initial diameter of ~50 nm to

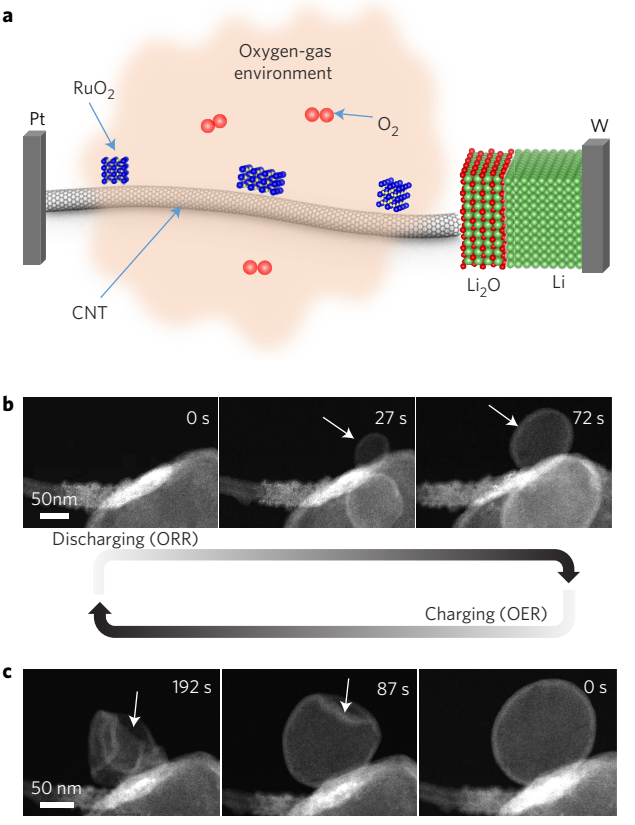

Figure 1 | *In situ* observation of the morphological evolution of the discharge/charge product. a, Schematic that illustrates the configuration of the Li-O_2 nanobattery in an environmental TEM chamber. A CNT dressed with RuO_2 (cathode) mounted on a Pt tip is connected with a Li_2O-covered Li metal on a W tip, which is exposed to an O_2 environment. **b**, The time-resolved high-angle annular dark-field scanning TEM images depict the morphological evolution of the discharging product (ORR), which features the nucleation and growth of a hollow nanostructure (white arrows). **c**, The images illustrate the morphological evolution on charging (OER), which features the collapsing of the hollow nanostructure (white arrows).

[1]Environmental Molecular Sciences Laboratory, Pacific Northwest National Laboratory, 902 Battelle Boulevard, Richland, Washington 99352, USA. [2]Energy and Environment Directorate, Pacific Northwest National Laboratory, 902 Battelle Boulevard, Richland, Washington 99352, USA. [3]School of Environmental and Chemical Engineering, Tianjin Polytechnic University, Tianjin 300387, China. *e-mail: chongmin.wang@pnnl.gov

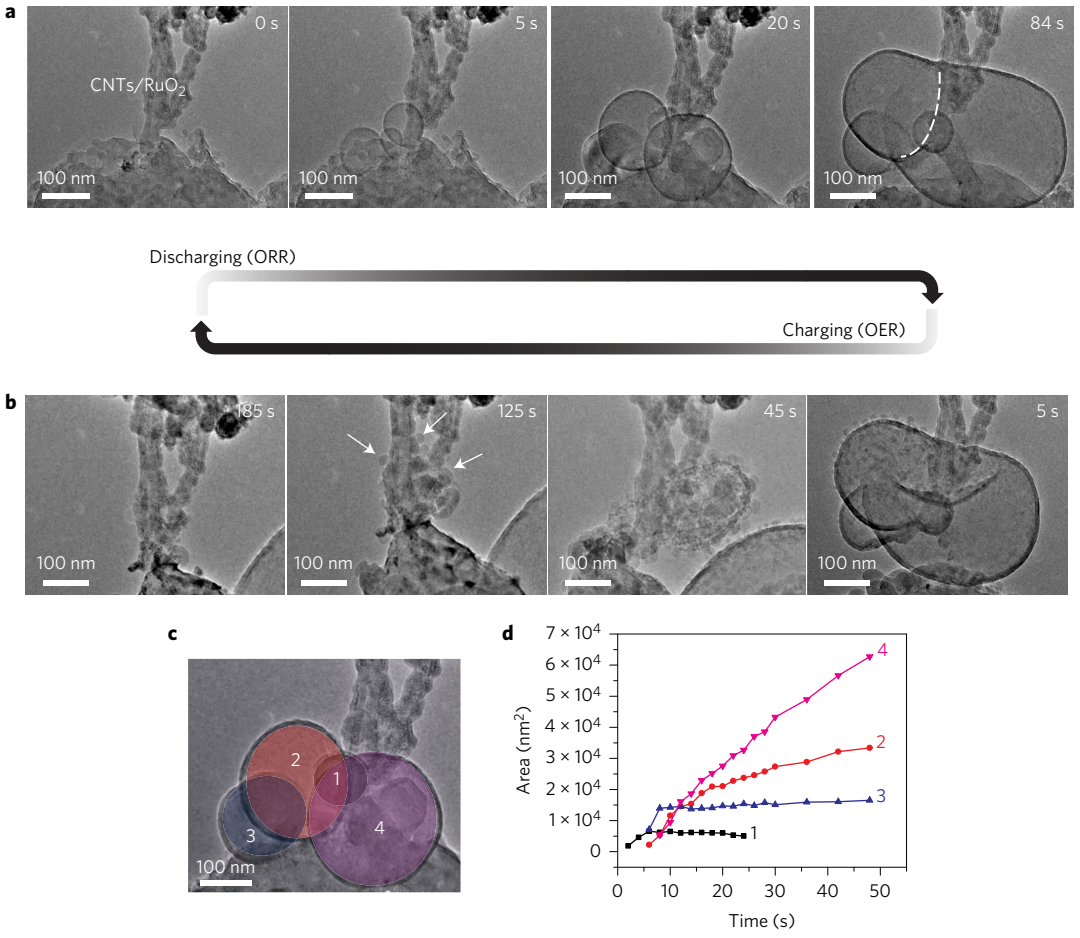

Figure 2 | *In situ* TEM observation of the morphological evolution of the discharge–charge products. a,**b**, Time-resolved *in situ* TEM images show the nucleation and growth of hollow spherical particles during the discharging process, which corresponds to the ORR, and the impingement of two growing particles leads to the formation of a boundary between them, as illustrated in the image of 84 s by the dashed line (**a**); on charging, which corresponds to the OER, the hollow spherical particle decomposes, which leads to the collapse of the spherical particles and the formation of small particles (white arrows) (**b**). **c**,**d**, The projected area of four hollow particles (labelled as 1–4 in **c**) as a function time is shown in **d**, which reveals a typical diffusion-controlled growth.

~200 nm during the ORR. On charging (Fig. 1c), the hollow sphere shrank and collapsed to a crumpled shell within a few minutes during the oxygen-evolution reaction (OER). The collapse of the hollow spheres features a sudden inward contraction of the shell from a single location, which leads to a unique morphology, as frequently observed after a partial charge (Fig. 1c). The expansion and shrinkage of the hollow spherical particle on the cathode during the battery cycling was further verified by TEM imaging (Supplementary Movie 2), in which a more-detailed structure can be obtained because of a faster temporal resolution than in scanning TEM high-angle annular dark-field images. As representatively shown by the time-resolved TEM images in Fig. 2a, sequential nucleation and growth of hollow spheres were observed at multiple locations on the CNTs. A contact of two growing hollow spheres can lead to the coalescence of spheres, which is visible in the image at 84 s in Fig. 2a (the interface between two spheres is marked by the white dashed line). On charging, the decomposition process proceeds through the formation of small particles at the expense of the large hollow spherical particle (Fig. 2b). Quantification of the growth rates of the spheres indicates that this is a diffusion-limited process (Fig. 2c,d).

But why does the reaction product form a hollow sphere, instead of solid particles or a layered structure? To answer this question, we used *in situ* selected-area electron diffraction (SAED) analysis to provide chemical information on the phase evolution during the discharging and charging processes. For the solid-state oxygen-rich environment, LiO_2 is the initial discharging product, which subsequently evolves into Li_2O_2 and O_2 through a disproportionation reaction. It is simply the spatial location of this disproportionation reaction that leads to the trapping of the released O_2 inside the particle and subsequently inflates the particle to a hollow structure. As shown in Fig. 3a, during the first few seconds only crystalline LiO_2 and polycrystalline Li_2O can be seen from the SAED patterns. The Li_2O_2 emerged after ~30 s and coexisted with LiO_2. After 100 s, diffraction spots from LiO_2 gradually disappeared and the final product is polycrystalline Li_2O_2 and Li_2O. TEM dark-field imaging (Supplementary Fig. 2a,b) indicates that the LiO_2 is spatially located in the inner shell of the hollow sphere. Comparison of the SAED patterns (Supplementary Fig. 2c,d) between a fully formed hollow sphere and a residual shell after partial charging also shows that the outer shell is Li_2O and the inner shell is Li_2O_2. On charging, as shown in Fig. 3c, the intensity of the diffraction spots attenuates with time for both Li_2O and Li_2O_2. In the image at 48 s, two diffraction spots from LiO_2 emerge and do not appear in the image of 120 s, which indicates the LiO_2 can also be formed as an intermediate phase during the decomposition of Li_2O_2. Our observation of a metastable LiO_2 species appears to be consistent with the work of Lu *et al.*[17], in which, for an Li–O_2 battery using a graphene-supported Ir catalyst, the stabilization of LiO_2 is achieved through the lattice matching between Ir and LiO_2.

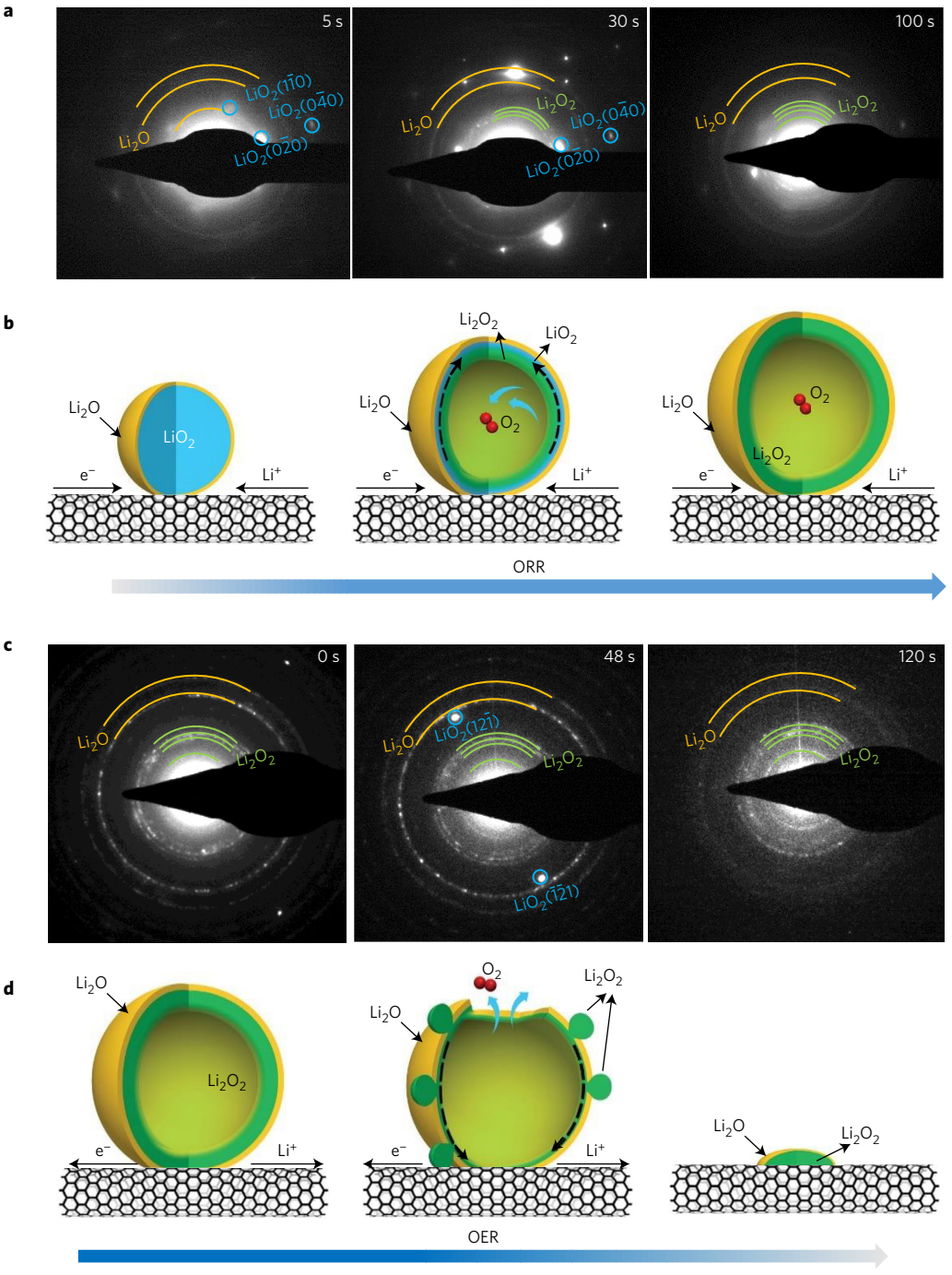

Figure 3 | *In situ* SAED analysis of phase evolution and the corresponding coupled reaction mechanisms. a,**b**, Time-resolved SAED patterns illustrate the case of discharging, in which LiO_2 is formed and subsequently evolves into Li_2O_2 and O_2 through a disproportionation reaction and the O_2 gas inflates the particle to a hollow structure (**a**), as illustrated schematically in **b**; the dashed arrows indicate the mass and charge-transfer direction. **c**,**d**, Time-resolved SAED patterns illustrate the case of charging, in which Li_2O_2 decomposes, that leads to the collapse of the hollow spherical particles (**c**), as schematically illustrated in **d**; the dashed arrows indicate the mass and charge-transfer direction.

Our observations provide clues to elucidate the pathway of the formation/decomposition of the discharging product on CNTs in the solid-state environment (Fig. 3b,d). On discharging, Li^+ ions diffuse across the electrolyte to react with oxygen at the three-phase junction to form LiO_2 ($O_2 + Li^+ + e^- \rightarrow LiO_2$). Owing to its metastable nature, LiO_2 is subsequently subjected to a disproportionation reaction, $LiO_2 \rightarrow Li_2O_2 + O_2$, which leads to the formation of Li_2O_2 and the release of O_2 gas. This reaction is a chemical reaction rather than an electrochemical one, for it can proceed rapidly without any electron-transfer event. As the surface diffusion of Li^+ ions is the most-effective route under solid-state conditions, the surface of LiO_2 can form Li_2O in the presence of an excess of Li^+ through the reaction $O_2 + 4Li^+ + 4e^- \rightarrow 2Li_2O$. Although the outer surface is passivated with Li_2O, the released O_2 gas inflates the hollow spheres (Figs 1b,c and 2a,b), which can increase from an initial size of ~10 nm to ~100 nm in diameter (Supplementary Information). Clearly, the growth of a hollow spherical particle is not a process that corresponds to a plastic deformation of a pre-existing solid particle of any significant dimension; rather, it is a process that is sustained by the continuous formation of LiO_2

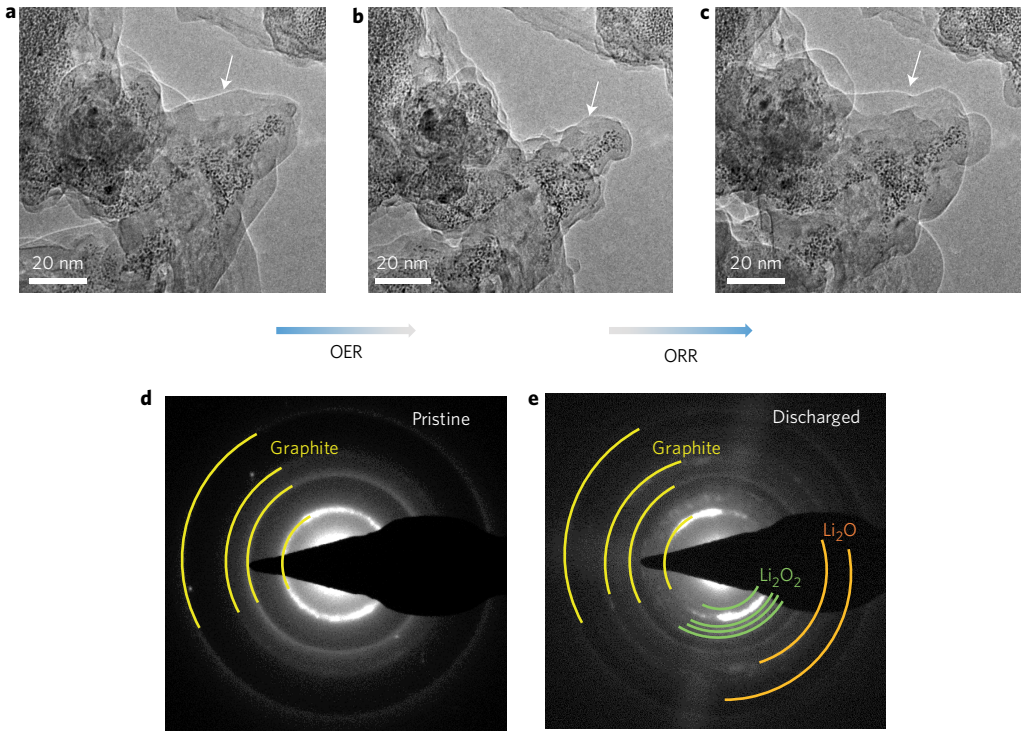

Figure 4 | Conformal coatings of discharging product. a–c, *In situ* TEM images show morphological changes on the surface of CNTs during the first OER and the second ORR feature the decomposition and formation of a conformal coating layer on the carbon surface with charging and discharging (white arrows). **d**,**e**, SAED patterns of pristine CNT/RuO_2 (**a**) and discharged CNT/RuO_2 (**b**) reveal that the conformal coatings formed on the carbon surface are Li_2O_2 and Li_2O.

and Li_2O at the site where the Li^+ ions, electrons and oxygens meet and subsequently feed to the inner side as LiO_2 and to the outside as Li_2O, because the Li_2O outer layer also expands without cracking. This indicates the particle growth is sustained by continuous mass transport to the shell of the hollow particle, which is also evidenced by an increase in the average shell thickness from 5.2 nm at 27 s to 12.2 nm at 72 s (Fig. 1b). On charging, Li_2O_2 loses one Li^+ and one electron to form LiO_2 ($Li_2O_2 \rightarrow LiO_2 + Li^+ + e^-$), which then releases O_2 gas until complete decomposition. A direct decomposition of Li_2O_2 is also possible, but cannot be confirmed by our experiments. Morphologically, the formation of small particles, rather than the direct decomposition of the large hollow particle, results from their overall higher surface area, which leads to a fast decomposition (Fig. 2b) and indicates that the OER is kinetically favoured through this process. This is in accordance with the fact that charging takes longer than discharging (Figs 1 and 2).

Although the hollow spheres are the major discharging product of the Li–O_2 battery, a conformal coating layer also forms (Fig. 4a–c and Supplementary Movie 3). As indicated in Fig. 4d,e, the SAED analysis reveals the co-existence of both Li_2O and Li_2O_2 in the conformal coating layer. Similar to the decomposition of the hollow-sphere particle described in Fig. 2b, the decomposition of the conformal layer during the OER was observed to proceed through the nucleation of small particles accompanied by the releasing of O_2 gas (Supplementary Movie 4). Unlike the large hollow spheres that decompose completely on charging, the conformal coatings on the CNT surface cannot be removed completely, and leave a residual layer a few nanometres thick (Fig. 4b).

To confirm the Li–O_2 chemistry described above, we also found that using a pure CNT cathode shows the formation of hollow spheres, and when H_2O vapour is introduced instead of O_2, the hollow spherical particles do not form (Supplementary Information).

The complete reaction pathways for Li–O_2 in a solid-state environment revealed above resemble that postulated for an aprotic system. There are, however, important differences. First, a solid-state reaction pathway requires no intermediate superoxide radical anion ($O_2^{\bullet-}$). Second, the large particles of discharging product can be formed on the surface of CNTs through surface diffusion of Li^+ rather than just on the three-phase junctions, as has been generally believed. This argument is consistent with the observation that the formation/decomposition process of the hollow spheres takes place not only on the three-phase junction, but also at other locations on the CNTs (Supplementary Fig. 3). Third, it has been postulated that the large particles can only grow through a precipitation route in the solution[15,18,19]. However, the observation that the hollow spheres can grow to a large size indicates the morphology of the discharging product is independent of its fundamental reaction pathways, but determined by the close coupling of the diffusion of Li^+ ion, electron transport and reaction sites, as well as by the spatial accommodation of the reaction products.

Also, our findings provide insights for the understanding of aprotic systems. The formation of a toroidal particle[20] is proposed to be triggered by the presence of solvent (water) and that $O_{2(sol)}^-$ acts as a redox shuttle[18]. The toroid structure results from the fact that the growing particle should enable a shorter (compared with the carbon surface) second path for electron diffusion and also facilitate oxygen-gas release during the disproportionation reaction. This is similar to a solid-state environment in which surface diffusion of Li^+/electron and the release of O_2 are both enabled by hollow spherical particles, which in turn self-limit their own growth through surface diffusion. For the case of an aprotic Li–O_2 battery, Jung *et al.*[21,22] also noticed the formation of hollow spherical particles in the discharged product. The formation of a hollow spherical particle during the discharge process using both liquid and solid electrolytes indicates that similar Li^+- and electron-diffusion conditions can exist for both electrolytes, that is, insufficient wetting of the cathode materials in liquid electrolyte. Also, the presence of a Li_2O phase in the discharging product may be unique for a

solid-state environment in which O_2 gas is in surplus and in direct contact with the discharging product, and so leads to the formation of a surface layer of Li_2O.

In conclusion, we have identified the full reaction pathway for a solid-state Li–O_2 battery that features a transient disproportionation chemical reaction of LiO_2 into Li_2O_2 with the release of O_2 and the formation of a hollow structured particle during discharge, and with a two-step decomposition of the Li_2O_2 hollow particles (collapse of the shell and nucleation of smaller particles) during charge. The close coupling of Li^+ diffusion, electron transport, reaction site and the accommodation of released O_2 gas governs the formation of the complex morphological features observed during discharge. Although the morphology of the discharging product varies for solid-state (hollow sphere) and aprotic (toroid) systems, the phase of the reaction product is identical for both batteries. We believe that our *in situ* method can also provide insights to other electrochemical catalytic reactions.

Methods

Methods and any associated references are available in the online version of the paper.

Received 21 September 2016; accepted 31 January 2017; published online 27 March 2017

References

1. Girishkumar, G., McCloskey, B., Luntz, A. C., Swanson, S. & Wilcke, W. Lithium–air battery: promise and challenges. *J. Phys. Chem. Lett.* **1,** 2193–2203 (2010).
2. Christensen, J. *et al.* A critical review of Li/air batteries. *J. Electrochem. Soc.* **159,** R1–R30 (2011).
3. Bruce, P. G., Freunberger, S. A., Hardwick, L. J. & Tarascon, J.-M. Li–O_2 and Li–S batteries with high energy storage. *Nat. Mater.* **11,** 19–29 (2012).
4. Lu, Y.-C. *et al.* Lithium–oxygen batteries: bridging mechanistic understanding and battery performance. *Energy Environ. Sci.* **6,** 750–768 (2013).
5. Shao, Y. *et al.* Making Li–air batteries rechargeable: material challenges. *Adv. Func. Mater.* **23,** 987–1004 (2013).
6. Balaish, M., Kraytsberg, A. & Ein-Eli, Y. A critical review on lithium–air battery electrolytes. *Phys. Chem. Chem. Phys.* **16,** 2801–2822 (2014).
7. Lu, J. *et al.* Aprotic and aqueous Li–O_2 batteries. *Chem. Rev.* **114,** 5611–5640 (2014).
8. Luntz, A. C. & McCloskey, B. D. Nonaqueous Li–air batteries: a status report. *Chem. Rev.* **114,** 11721–11750 (2014).
9. Peng, Z. *et al.* Oxygen reactions in a non-aqueous Li^+ electrolyte. *Angew. Chem. Int. Ed.* **50,** 6351–6355 (2011).
10. Aurbach, D., McCloskey, B. D., Nazar, L. F. & Bruce, P. G. Advances in understanding mechanisms underpinning lithium–air batteries. *Nat. Energy* **1,** 16128 (2016).
11. Laoire, C. O., Mukerjee, S., Abraham, K. M., Plichta, E. J. & Hendrickson, M. A. Influence of nonaqueous solvents on the electrochemistry of oxygen in the rechargeable lithium–air battery. *J. Phys. Chem. C* **114,** 9178–9186 (2010).
12. Allen, C. J. *et al.* Oxygen reduction reactions in ionic liquids and the formulation of a general ORR mechanism for Li–air batteries. *J. Phys. Chem. C* **116,** 20755–20764 (2012).
13. Trahan, M. J., Mukerjee, S., Plichta, E. J., Hendrickson, M. A. & Abraham, K. M. Studies of Li–air cells utilizing dimethyl sulfoxide-based electrolyte. *J. Electrochem. Soc.* **160,** A259–A267 (2013).
14. McCloskey, B. D., Scheffler, R., Speidel, A., Girishkumar, G. & Luntz, A. C. On the mechanism of nonaqueous Li–O_2 electrochemistry on C and its kinetic overpotentials: some implications for Li–air batteries. *J. Phys. Chem. C* **116,** 23897–23905 (2012).
15. Johnson, L. *et al.* The role of LiO_2 solubility in O_2 reduction in aprotic solvents and its consequences for Li–O_2 batteries. *Nat. Chem.* **6,** 1091–1099 (2014).
16. Huang, J. Y. *et al. In situ* observation of the electrochemical lithiation of a single SnO_2 nanowire electrode. *Science* **330,** 1515–1520 (2010).
17. Lu, J. *et al.* A lithium–oxygen battery based on lithium superoxide. *Nature* **529,** 377–382 (2016).
18. Aetukuri, N. B. *et al.* Solvating additives drive solution-mediated electrochemistry and enhance toroid growth in non-aqueous Li–O_2 batteries. *Nat. Chem.* **7,** 50–56 (2015).
19. Gao, X., Chen, Y., Johnson, L. & Bruce, P. G. Promoting solution phase discharge in Li–O_2 batteries containing weakly solvating electrolyte solutions. *Nat. Mater.* **15,** 882–888 (2016).
20. Mitchell, R. R., Gallant, B. M., Thompson, C. V. & Shao-Horn, Y. All-carbon-nanofiber electrodes for high-energy rechargeable Li–O_2 batteries. *Energy Environ. Sci.* **4,** 2952–2958 (2011).
21. Jung, H.-G., Hassoun, J., Park, J.-B., Sun, Y.-K. & Scrosati, B. An improved high-performance lithium–air battery. *Nat. Chem.* **4,** 579–585 (2012).
22. Jung, H.-G. *et al.* A transmission electron microscopy study of the electrochemical process of lithium–oxygen cells. *Nano Lett.* **12,** 4333–4335 (2012).

Acknowledgements

This work is supported by the Assistant Secretary for Energy Efficiency and Renewable Energy, Office of Vehicle Technologies of the US Department of Energy under Contract no. DE-AC02-05CH11231, Subcontract no. 18769 and DE-AC-36-08GO28308 under Advanced Batteries Materials Research. The work was conducted in the William R. Wiley Environmental Molecular Sciences Laboratory, a national scientific user facility sponsored by the Department of Energy (DOE) Office of Biological and Environmental Research and located at the Pacific Northwest National Laboratory (PNNL). PNNL is operated by Battelle for the DOE under Contract DE-AC05-76RLO1830.

Author contributions

L.L., W.X., J.-G.Z. and C.M.W. conceived the experiment, B.L. and S.D.S. prepared the sample, L.L. carried out the *in situ* experiments, C.M.W. led the project and L.L. and C.M.W. wrote the manuscript with input from all the authors.

Additional information

Supplementary information is available in the online version of the paper. Reprints and permissions information is available online at www.nature.com/reprints. Correspondence and requests for materials should be addressed to C.W.

Competing financial interests

The authors declare no competing financial interests.

Methods

Materials preparation. Multiwalled CNTs (Cheap Tubes Inc.) were cast into a 0.1 M ruthenium(III) chloride hydrate (Sigma-Aldrich) solution followed by ultrasonication. After 15 h of stirring, the precipitation was washed several times with distilled water, and then vacuum dried. Finally, black CNT/RuO_2 powders were obtained after a thermal treatment at 150 °C.

***In situ* environmental TEM of the Li–O_2 nanobattery system.** The solid-state nanobattery was constructed through a two-probe configuration. The CNT/RuO_2 cathode was loaded on a Pt probe, and brought to a Li_2O-covered Li metal anode anchored on the other tungsten probe through precise a nanomanipulation inside the environmental TEM. The oxygen-gas environment around the sample was maintained at a pressure of 0.1 mbar throughout the *in situ* experiments. The electrochemical reaction is driven by external biasing, that is, a negative bias applied at the Pt end to drive the Li^+ to cross the Li_2O layer to react with oxygen, which corresponds to the ORR during the discharging of the Li–O_2 battery; a positive bias drives the Li^+ ions back to the Li_2O/Li end, which leads to the decomposition of the discharged product, an OER during the charging of the battery. Real-time visualization of the structural and phase changes of the air cathode in a working Li–O_2 battery can be correlated directly to the electrochemical reactions based on the above configuration.

Data availability. The data that support the plots within this paper and other findings of this study are available from the corresponding author on reasonable request.